

Power-Efficiency Constraint for Chemical Motors

R. X. Zhai¹ and Hui Dong^{1,*}

¹Graduate School of China Academy of Engineering Physics, Beijing, 100193, China

(Dated: April 1, 2025)

Chemical gradients provide the primordial energy for biological functions by driving the mechanical movement of microscopic engines. Their thermodynamic properties remain elusive, especially concerning the dynamic change in energy demand in biological systems. In this article, we derive a constraint relation between the output power and the conversion efficiency for a chemically fueled steady-state rotary motor analogous to the F_0 -motor of ATPase. We find that the efficiency at maximum power is half of the maximum quasi static efficiency. These findings shall aid in the understanding of natural chemical engines and inspire the manual design and control of chemically fueled microscale engines.

I. INTRODUCTION

As a counterpart to heat engines [1], chemical engines are fueled by chemical reactions, converting chemical energy into mechanical work [2–8]. These engines, such as the Kinesin and ATP synthase, are ubiquitous in open systems like living organisms and play crucial roles [9–12]. Recently, the thermodynamic behavior of these engines, together with the related chemical processes, has garnered significant attention [5, 8, 13–18], especially on the power-efficiency trade-off of chemical engines in finite time due to the substantial varying energy consumption rate in biological systems.

Efficiency, which measures the conversion ratio of free energy to mechanical work, is a core parameter of thermodynamic engines. However, the optimal efficiency is typically achieved only when the cycle time approaches infinity resulting in a zero power output [19–23], which is another critical parameter for assessing the performance of chemical engines. The pursuit of non-zero power inevitably leads to a decrease in efficiency, making the trade off [24–31] between power and efficiency a significant topic in finite-time thermodynamics [32, 33]. For chemical engines, quantitatively studying the power-efficiency constraint will establish performance boundaries, aiding in the understanding of natural chemical engines [7, 34–40] and inspiring the manual design and control of microscale engines fueled by chemical reactions [8, 14, 15, 17, 41].

In this article, we investigate a rotary motor fueled by chemical reactions, resembling the F_0 motor of ATP synthase [9–11]. We use thermodynamic cycles to describe the operation of such steady-state engine, which interacts with two reservoirs with different chemical potentials, performing mechanical work through its autonomous rotation. Its power and efficiency are regulated by its rotation speed and an inside potential. Our analysis reveals the power-efficiency constraint relation for this chemical engine. When the chemical potential difference between the two reservoirs is small, this constraint takes a simple analytical form. Interestingly, in this regime, the ra-

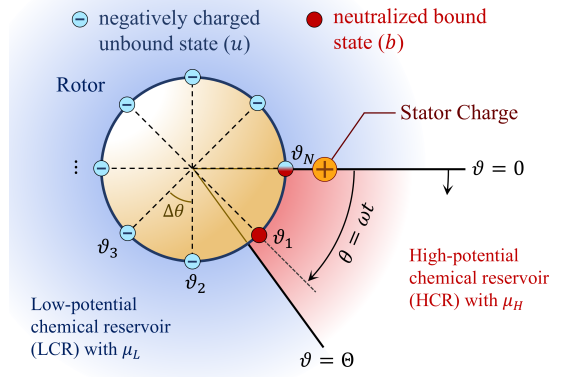


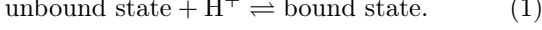
Figure 1. The rotary motor model consisting of a rotor and a stator. The rotor has a ring structure composed of multiple c-subunits, depicted by yellow blocks. Each subunit contains a negatively charged ionic binding site with the light blue representing the unbound state (u) with negative charge and dark red as the neutralized bound state (b). The rotation coordinate of the rotor is denoted as θ , where a clockwise rotation is defined as the positive direction. The stator interacts with the rotor through a fixed charge, represented by the large orange circle, located at $\theta = 0$. This charge provides an attractive inside potential $\Phi(\theta)$ for the negatively charged sites. The motor interacts with a high chemical potential (μ_H) reservoir (HCR) (red shaded region) with the angular width Θ , and a low chemical potential (μ_L) reservoir (LCR) (blue shaded region).

tio between efficiency at maximum power and the upper limit of efficiency is $1/2$, a coefficient that appears to be universal for thermodynamic cycles in the linear response regime.

II. MODEL OF BIOLOGICAL ROTARY MOTOR

Fig. 1 illustrates the current rotary motor, consisting of a rotor and a stator. The rotor comprises N negatively charged binding sites, which are evenly distributed along a circular ring. The charge of these sites can be neutralized by binding with one positively charged ion from the reservoirs, as described in the following chemi-

cal reaction:



The light blue and dark red colors on these sites correspond to the neutralized bound state (denoted by b) and negatively charged unbound state (denoted by u) respectively.

For the j -th binding site, its position ϑ_j is obtained by $\vartheta_j = \theta + (j - 1)\Delta\theta$, where $\Delta\theta = 2\pi/N$. The parameter θ represents the position of the first site and can also serve as the generalized coordinate of the rotor's overall rotation state. The state for all binding sites $(s_1, \dots, s_N) = b, u$, together with the coordinate θ , constitute the configuration space for the rotor $(\{s_j\}, \theta)$.

When the motor achieve its steady state, the force generated by the rotor at steady rotation is approximately constant due to the dense and evenly-spaced binding sites, and is balanced by a constant load and the friction, inducing a constant rotation speed $\dot{\theta} = \omega$. Under this approximation, all binding sites exhibit identical temporal evolution, aside from a phase delay. Consequently, studying the thermodynamic cycle of one specific binding site, e.g., the first site, is sufficient to reflect the behavior of the whole motor. For example, the work for the whole motor during a complete cycle is obtained by multiplying the work from one site with the number N . Our subsequent analysis will focus on the thermodynamic cycle of the first binding site, whose configuration space is expressed as (s, θ) .

For the site of interest, its energy $U(u, \theta)$ in the unbound state u is determined by an inside potential $\Phi(\theta)$ due to the Coulomb interaction between its charge and a fixed charge (the large orange circle) on the stator located at $\vartheta_0 = 0$, namely $U(u, \theta) = \Phi(\theta)$. We apply the Coulomb interaction to determine the form of $\Phi(\theta)$, which is presented in Appendix A. The energy $U(b, \theta)$ for the site in the bound state b is given only by the binding energy E_b without the Coulomb interaction, namely $U(b, \theta) = E_b$.

The motor is in contact with two chemical reservoirs: a high chemical potential reservoir (HCR) with chemical potential μ_H (red shadowed region around the motor) and a low chemical potential reservoir (LCR) with chemical potential μ_L (blue shadowed region around the motor). Thus, the environmental chemical potential for the binding site of interest $\mu(\theta)$ is expressed as a function of its position θ , i.e., $\mu(\theta) = \mu_H$ for $0 \leq \theta < \Theta$, and $\mu(\theta) = \mu_L$ for $\Theta < \theta \leq 2\pi$. Here, Θ is the angular width of the HCR. During the rotation, the binding sites alternate their contact between the high and low potential reservoirs.

We denote for the site of interest the average binding number in the bound state b as n ($0 \leq n \leq 1$). When the site is in equilibrium with a reservoir, the average binding number $n = n^{(0)}$ is determined by the energy

decrease $\Delta U(\theta) = E_b - \Phi(\theta) - \mu(\theta)$ of reaction (1), as

$$n^{(0)}(\theta) = \frac{1}{1 + e^{\beta \Delta U(\theta)}}, \quad (2)$$

where $\beta = (k_B T)^{-1}$ is the inverse temperature of the reservoirs. For finite-time processes, the evolution of n is determined by the rate equation [13] of reaction (1), and the change rate of the average binding number n is proportional to its difference from the equilibrium, i.e., $\dot{n} = -(n - n^{(0)})/\tau_r$, where τ_r is the timescale of relaxation between the binding site and the reservoir. Here, we have assumed the same timescale τ_r for the relaxation in the two chemical reservoirs. Replacing the variable t with the angular coordinate $\theta = \theta_0 + \omega t$, we obtain the evolution equation of $n(\theta)$ as

$$\frac{dn}{d\theta} = -\frac{1}{\omega \tau_r} (n - n^{(0)}(\theta)), \quad (3)$$

with a periodic boundary condition $n(\theta) = n(\theta + 2\pi)$, the effect of finite operation time is characterized by the dimensionless coefficient $\omega \tau_r$.

III. POWER AND EFFICIENCY OF THE MOTOR

The average energy of one site is expressed with the average binding number as $F = nE_b + (1 - n)\Phi(\theta)$ with its change given by $dF = [E_b - \Phi(\theta)]dn + (1 - n)\Phi'(\theta)d\theta$. The first term is the energy change caused by the particle exchange with the reservoirs, and the second term represents the mechanical work $W_{\text{mech}} = \int_{-\pi}^{\pi} (1 - n)\Phi'(\theta)d\theta$. For rotation with a finite rotation speed ω , we introduce a linear dissipation $W_{\text{diss}} = 2\pi\gamma\omega$ to account for the energy loss due to friction. Here γ is the given linear friction coefficient accounting for the resistance torque proportional to the rotation speed ω . The net work output per cycle is obtained as $W_{\text{net}} = W_{\text{mech}} - W_{\text{diss}}$. The thermodynamic efficiency of the cycle is,

$$\eta = \frac{W_{\text{net}}}{\Delta\mu\Delta n}, \quad (4)$$

where $\Delta\mu = \mu_H - \mu_L$ is the chemical potential difference, and $\Delta n = n(\Theta) - n(0)$ is the average number of particles transferred from the HCR to the LCR. Here, $\Delta\mu\Delta n$ describes the free energy decrease for the chemical reservoirs due to the transport of Δn ions. The efficiency in Eq. (4) reflects the ratio of the net work output W_{net} with respect to the free energy decrease. The (average) power is obtained as the average mechanical energy output rate per cycle

$$P = \frac{W_{\text{net}}}{\tau_{\text{cycle}}}, \quad (5)$$

where $\tau_{\text{cycle}} = 2\pi/\omega$ is the cycle time.

IV. MAXIMUM QUASI-STATIC EFFICIENCY

In the quasi static limit with $\omega\tau_r \rightarrow 0$, the binding site keeps in equilibrium with the reservoir, and hence the average binding number is obtained by Eq. (2). The energy dissipated due to the friction W_{diss} is 0 in such quasi static limit. The net work output of a complete cycle for the quasi static limit is then obtained as

$$\begin{aligned} W_{\text{net}}^{(0)} &= - \int_0^{2\pi} (1 - n(\theta)) \Phi'(\theta) d\theta \\ &= - \oint (1 - n) d\Phi = \oint n d\Phi. \end{aligned}$$

In the $n - \Phi$ diagram shown in Fig. 2(a), the net work output is the area of the light blue shaded region enclosed by the blue solid line shown with $n(\theta), \Phi(\theta)$. The work output is obtained as

$$\begin{aligned} W_{\text{net}}^{(0)} &= k_B T \ln \frac{1 + e^{\beta(\Phi(0) - E_b + \mu_L)}}{1 + e^{\beta(\Phi(0) - E_b + \mu_H)}} \\ &\quad - k_B T \ln \frac{1 + e^{\beta(\Phi(\Theta) - E_b + \mu_L)}}{1 + e^{\beta(\Phi(\Theta) - E_b + \mu_H)}}. \end{aligned} \quad (6)$$

We conclude that the quasi static work is determined by the values of $\Phi(\theta)$ at the edges of the channel, i.e., $\Phi(0)$ and $\Phi(\Theta)$. The number of particles transferred in a quasi static cycle is given by

$$\Delta n^{(0)} = \frac{1}{1 + e^{-\beta(\Phi(\Theta) - E_b + \mu_H)}} - \frac{1}{1 + e^{-\beta(\Phi(0) - E_b + \mu_L)}}. \quad (7)$$

We first optimize E_b to get the maximum quasi static efficiency $\eta^{(0)}$ as derived from Eq. (4), by requiring that $\partial\eta^{(0)}/\partial E_b = 0$. The optimum E_b is obtained as

$$E_b = \frac{\mu_H + \mu_L + \Phi(\Theta) + \Phi(0)}{2},$$

with which the quasi static efficiency is maximized as

$$\eta_{\text{max}}^{(0)} = \frac{1 + \cosh(\beta\Delta_+/2)}{\beta\Delta\mu \sinh(\beta\Delta_+/2)} \ln \left(\frac{1 + \cosh(\beta\Delta_+/2)}{1 + \cosh(\beta\Delta_-/2)} \right), \quad (8)$$

where $\Delta_+ \equiv V + \Delta\mu$, $\Delta_- \equiv V - \Delta\mu$, and $V \equiv \Phi(\Theta) - \Phi(0)$ defines the inside potential depth. In the quasi static limit, the detailed shape of the internal potential $\Phi(\theta)$ is irrelevant, and only inside potential depth (IPD) V determines the overall efficiency of the cycle. The upper limit of quasi static efficiency in Eq. (8) is obtained as 1 with $V \rightarrow \infty$ or $\Delta\mu \rightarrow 0$, representing that all the free energy drawn from the HCR is converted into mechanical work. For further discussions about these limits, please see Appendix B. Such quasi static cycles are impractical for biological systems, since the power output is 0 noting that the cycle time τ_{cycle} is infinite.

V. CONSTRAINT BETWEEN POWER AND EFFICIENCY

To acquire a finite output power, the motor rotates with a non-zero rotation speed ω . The finite time behavior of the motor is numerically evaluated in Fig. 2. The blue solid curves illustrate the quasi static cycle, while the green dashed curves, the red dash-dotted curves and the black dotted curves illustrate cycles with rotation speeds $\omega\tau_r = \Theta/5$, $\Theta/2$ and $5\Theta/3$, respectively. In Fig. 2 (a), the $n - \Phi$ diagrams are plotted. It is evident that the mechanical work decreases with an increase in ω . We note that for large ω , e.g., $\omega\tau_r = 5\Theta/3$, the total work output W_{net} becomes negative, which means the motor no longer works as an engine. In the following discussion, we only consider the situation with positive output work $W_{\text{net}} > 0$.

The effect of such finite time operation will induce not only smaller mechanical work, but also larger frictional dissipation W_{diss} . In Fig. 2 (b) and (c), the curves show the average binding number $n(\theta)$ (in Fig. 2(b)) and the cumulative net work output $W_{\text{net}}(\theta) = \int_{-\pi}^{\theta} (dW_{\text{mech}} - dW_{\text{diss}})$ (in Fig. 2(c)) as functions of the rotational coordinates θ for the range of $-\pi < \theta \leq \pi$. The red-shaded region in Figs. (b-c) illustrates the range where the binding site is in contact with the HCR. With increasing rotation speed ω , the relaxation processes in the two chemical potential reservoirs become inadequate. And in turn, this results in the decrease in the total net output work. In the calculation, we set the width $\Theta = \pi/5$ and the dissipation coefficient $\gamma = 0.5k_B T\tau_r$.

With the decrease of $\Delta\mu$, the mechanical work becomes smaller. Thus, to maintain a positive work output, ω should also decrease to reduce the dissipation. In such linear response (LR) regime with both $\Delta\mu$ and $\omega\tau_r$ are infinitesimal, the net work output and the exchanged particle number are expressed with series in ω and $\Delta\mu$. Up to the second order of $\Delta\mu$, the upper bound of finite time power output is obtained approximately as

$$P \leq 4P_{\text{max}}\eta(1 - \eta). \quad (9)$$

where the maximum power (MP) P_{max} reads

$$P_{\text{max}} = \frac{\Delta\mu^2}{8\pi} \max \left(\frac{[\Omega^{(0)}(V)]^2}{2\pi\gamma + \Lambda^{(0)}(V)\tau_r/\beta} \right). \quad (10)$$

Here $\Omega^{(0)}(V)$ and $\Lambda^{(0)}(V)$ are functions of the IPD V . The detailed derivation for this solution is shown in Appendix C. This relation characterizes the universal constraint between the power and efficiency of our motor within the LR regime. The corresponding efficiency, typically known as the efficiency at maximum power (EMP) $\eta_{\text{MP}} = 1/2$ is half of the maximum efficiency, being independent of the detailed parameters and configuration of

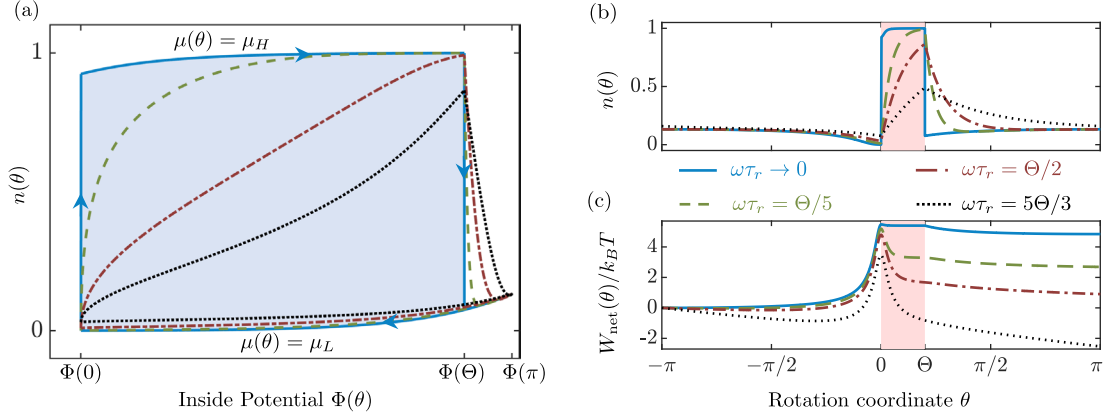


Figure 2. The thermodynamic cycle of our biological rotary motor. (a) $n - \Phi$ diagram for the motor. The area of the blue shaded region reflects the mechanical work output for the quasi static cycle. (b-c) Average binding number n and the cumulative net work output W_{net} as functions of θ within finite operation time. The red shaded region ($0 \leq \theta < \Theta$) represents the range where the site is in contact with the high potential chemical reservoir. The horizontal coordinates are the same for the two subfigures. The parameters are fixed as follows: $\Theta = \pi/5$, $V = 5k_B T$, $\Delta\mu = 10k_B T$, and $\gamma = 0.5\tau_r k_B T$. The blue solid curve shows the evolution in the quasi static limit with $\omega \rightarrow 0$. The green dashed curves, red dash-dotted curves and black dotted curves show the evolution with $\omega\tau_r = \Theta/5, \Theta/2, 5\Theta/3$, respectively. The increase in rotation speed causes a decrease in total work output per cycle, which is reflected by the final value of the curves $W_{\text{net}}(\pi)$. It is noteworthy that for $\omega\tau_r = 5\Theta/3$, the total work output W_{net} becomes negative, which means the motor no longer works as an engine.

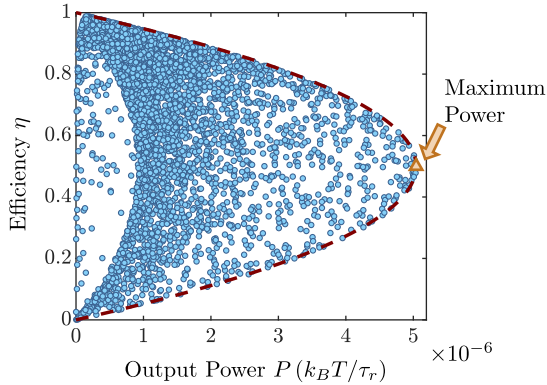


Figure 3. The constraint between the output power P and the efficiency for $\Delta\mu = 0.1k_B T$. We randomly evaluate 10^4 cycles with different combinations of rotation speed and IPD (ω, V), whose power and efficiency are shown with blue circles. The constraint relation within the LR regime is illustrated by the region enclosed by the dark dashed curve. The MP point with $P_{\text{max}} = 5.04 \times 10^{-6} k_B T/\tau_r$ and $\eta_{\text{MP}} = 0.50$ is indicated by the orange triangle.

the motor. The coefficient $1/2$ appears to be universal in the LR regime for all thermodynamic cycles [6, 20, 22, 42–45].

To validate our constraint relation in Eq. (9), we evaluate the efficiency and power by numerically solving Eq. (3) for different combinations of rotation speed and IPD (ω, V) with parameters $\Theta = \pi/5$, $\gamma = 5k_B T\tau_r$, and $\Delta\mu = 0.1k_B T$. The results of 10^4 random combinations with $0 < V/k_B T < 60$ and $0 < \omega < W^{(0)}/2\pi\gamma$ are illustrated as blue circles in Fig. 3. The constraint

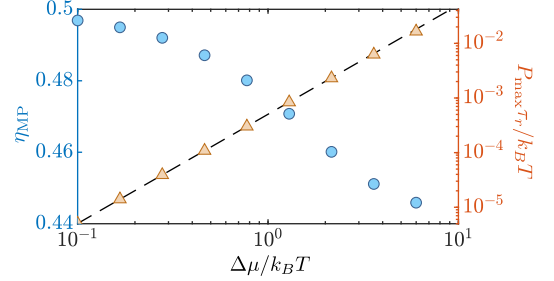


Figure 4. Efficiency at maximum power and maximum power within the linear response regime. As functions of the chemical gradient $\Delta\mu$, the efficiency at maximum power is illustrated with blue circles, and the maximum power is illustrated with yellow triangles. The dashed line shows the leading order proportional to $\Delta\mu^2$ of the maximum power.

relation in Eq. (9) is shown with the region enclosed by the dark red dashed curve. Within the LR regime, the data align well with the prediction, yielding the MP $P_{\text{max}} = 5.04 \times 10^{-6} k_B T/\tau_r$ and EMP $\eta_{\text{MP}} = 0.50$, indicated by the orange triangle.

To quantitatively evaluate the behavior outside the LR regime, we present the EMP (blue circles) and the MP (orange triangles) as functions of $\Delta\mu$ in Fig. 4 for $\Theta = \pi/5$ and $\gamma = 5k_B T\tau_r$. The dashed line shows the maximum power obtained from Eq. (10). The efficiency at maximum power η_{MP} decreases with increasing chemical gradient $\Delta\mu$, while the power increases with the increasing chemical gradients $\Delta\mu$. We note that the theoretical prediction in Eq. (10) for the LR regime also fits well with the simulation beyond the LR regime.

VI. CONCLUSION

We would like to mention that much attention has been drawn to the thermodynamic properties of the chemically fueled rotary engines, with most studies concentrating on the F_1 motor and the interaction between the F_1 and F_0 parts. Yet, the thermodynamic cycle for the F_0 portion is seldom explored, especially for its dynamic impact on power and efficiency. In this article, we have evaluated the constraint between the power and efficiency of a chemically fueled rotary motor operating at a steady rotation, considering various parameters such as the rotation speed, the depth of the inside potential and the friction coefficient. With the constraint relation, the maximum power and corresponding efficiency at maximum power are acquired. The efficiency at maximum power approaches $1/2$ in the linear response regime, which appears to be a universal coefficient for all finite-time thermodynamic cycles. We anticipate that this research will inspire further investigations into the thermodynamics of microscopic motors.

ACKNOWLEDGMENTS

R. X. Zhai is grateful to Y. H. Ma for his discussions. This work is supported by the Innovation Program for Quantum Science and Technology (Grant No. 2023ZD0300700) and the National Natural Science Foundation of China (Grants No. U2230203, No. U2330401, and No. 12088101).

Appendix A: Form of the inside Potential

In this appendix, we derive the form of the inside potential $\Phi(\theta)$ induced by the Coulomb interaction between the stator charge and the binding site. In Fig. 5(a), we denote the radius of rotor by R , and the distance between the stator charge and the center of the rotor by $(1+\delta)R$. The distance between the binding site and the stator charge with respect to the rotation coordinate θ is given by $r = R\sqrt{\delta^2 + 2(1-\cos\theta)\delta + 2(1-\cos\theta)}$. The potential energy of the Coulomb interaction between the stator charge and the unbounded binding site is

$$\Phi(\theta) = -\frac{\mathcal{E}}{r}. \quad (\text{A1})$$

where Φ_0 defines the potential energy at infinity, and $\mathcal{E} \equiv q_1 q_2 / (4\pi\epsilon)$ with q_1, q_2 as the charges for the binding site and stator charge, ϵ the permittivity of the medium. In the main text, we choose $\delta = 0.1$, and the parameter $\mathcal{E}(V)$ is determined by $\Phi(\Theta) - \Phi(0) = V$. The plot of the attractive inside potential $\Phi(\theta)$ is illustrated in Fig. 5(b) for $V = 5k_B T$. The red shaded region ($0 \leq \theta < \Theta$)

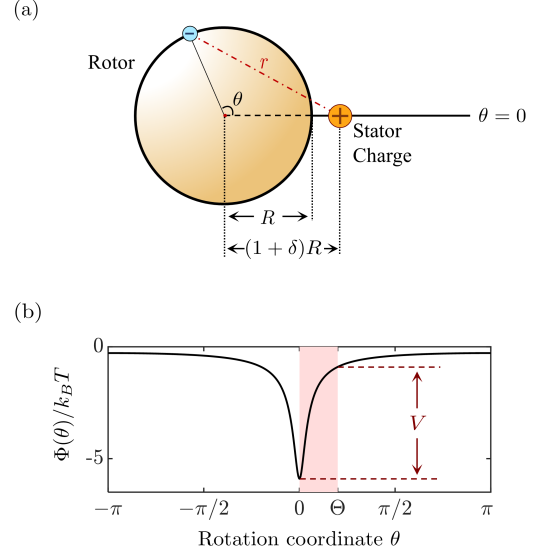


Figure 5. Inside potential of the biological motor. (a) A sketch of the structure of the microscopic rotor. The radius of the rotor is denoted by R , and the distance between the center of the rotor and the stator is $(1+\delta)R$. (b) The inside potential Φ as a function of the angular position θ . The potential $\Phi(\theta)$ is induced by the Coulomb interaction with a minimum at $\theta = 0$. The red shaded region represents the range where the site is in contact with the HCR. The inside potential depth is defined as the drop of Φ over this region, i.e., $\Phi(\Theta) - \Phi(0) = V$. In the plot, we have used parameters with the depth of the inside potential as $V = 5k_B T$ and $\Theta = \pi/5$.

represents the range where the site is in contact with the high potential chemical reservoir.

Appendix B: $n - \Phi$ Diagram for the quasi static cycles

In this appendix, we provide a detailed examination of the $n - \Phi$ diagram for quasi static cycles. In the $n - \Phi$ diagram, every point represents an equilibrium state of the binding site. The $n - \Phi$ diagrams for quasi static cycles under different values of $\Delta\mu$ are illustrated in Fig. 6(a) (the IPD is fixed as $V = 5k_B T$). The blue solid curves, green dashed curves, and red dash-dotted curves represent the $n - \Phi$ diagrams for $\Delta\mu = 10k_B T, 5k_B T$ and $0.5k_B T$, respectively (the chemical potential difference is fixed as $\Delta\mu = 10k_B T$). The $n - \Phi$ diagram for quasi static cycles under different values of IPD V are illustrated in Fig. 6(b). The blue solid curves, green dashed curves, and red dash-dotted curves represent the $n - \Phi$ diagrams for $V = 15k_B T, 10k_B T$ and $5k_B T$, respectively.

We show the $n - \Phi$ diagram for the case $\Delta\mu = 10k_B T$ (blue solid curve in Fig. 6(a)) as an example to describe the motor's cycling process. The thermodynamic cycle is

illustrated by the loop

$$A \rightarrow B \rightarrow C \rightarrow D \rightarrow E \rightarrow B \rightarrow A.$$

The processes of the cycle are described as follows:

- $A \rightarrow B \rightarrow C$: Iso-chemical potential process with $\mu = \mu_L$. In this process, the initial state A of the binding site corresponds to its position $\theta = -\pi$, and the final state C corresponds to $\theta = 0$.
- $C \rightarrow D$: Isometric relaxation with $\Phi = \Phi(0)$. In this process, the chemical potential of the binding site changes from μ_L to μ_H , combining with particles.
- $D \rightarrow E$: Iso-chemical potential process with $\mu = \mu_H$. During this process ($0 \leq \theta \leq \Theta$), the binding site is in contact with the HCR.
- $E \rightarrow B$: Isometric relaxation with $\Phi = \Phi(\Theta)$. In this process, the chemical potential of the binding site is changed from μ_H to μ_L , releasing particles.
- $B \rightarrow A$: Iso-chemical potential process with $\mu = \mu_L$. This process corresponds to the rotation from $\theta = \Theta$ to $\theta = \pi$, restoring the binding site from the state B to the initial state A .

The irreversibility during the quasi static cycles is caused by the relaxation processes $E \rightarrow B$ and $C \rightarrow D$, during which the site exchanges particles with a reservoir having a different chemical potential. When the chemical potential difference $\Delta\mu \rightarrow 0$ [shown in Fig. 6(a)], or the inside potential depth $V \rightarrow \infty$ [shown in Fig. 6(b)], the relaxation processes tend to vanish in the $n - \Phi$ diagram, resulting in the cycle being approximately reversible.

Appendix C: Power efficiency constraint relation in linear response regime

In this appendix, we consider the finite time behavior of the motor within the LR regime with $\Delta\mu \rightarrow 0$. In this situation, the rotation is slow enough to ensure a positive work output, i.e., $\omega\tau_r \rightarrow 0$, which will be validated as self-consistent later. Thus, we can approximate $n(\theta)$ with a series in terms of $\omega\tau_r$ as

$$n(\theta) = \sum_{k=0}^{\infty} \left(-\omega\tau_r \frac{d}{d\theta} \right)^k n^{(0)}(\theta),$$

which is a solution to Eq. (3). By keeping $\omega\tau_r$ to the first order, the function is obtained as

$$n(\theta) = n^{(0)}(\theta, \mu_H) - \frac{\omega\tau_r \beta e^{-\beta(E_b - \Phi(\theta) - \mu_H)}}{[1 - e^{-\beta(E_b - \Phi(\theta) - \mu_H)}]^2} \Phi'(\theta),$$

for $0 < \theta \leq \Theta$, and

$$n(\theta) = n^{(0)}(\theta, \mu_L) - \frac{\omega\tau_r \beta e^{-\beta(E_b - \Phi(\theta) - \mu_L)}}{[1 - e^{-\beta(E_b - \Phi(\theta) - \mu_L)}]^2} \Phi'(\theta),$$

for $\Theta < \theta \leq 2\pi$.

Within such an LR regime, the net work output and particle number exchange are expressed as series in ω and $\Delta\mu$, namely

$$\Delta n \approx \Delta n^{(0)} - \omega\tau_r \Delta n^{(1)}, \quad (C1)$$

$$W_{\text{net}} \approx W^{(0)} - \omega(2\pi\gamma + \tau_r W^{(1)}), \quad (C2)$$

with

$$\Delta n^{(0)} \approx \Omega^{(0)} + \Omega^{(1)} \beta \Delta\mu, \quad W^{(0)} = \Omega^{(0)} \Delta\mu,$$

$$\Delta n^{(1)} \approx \left(\Omega^{(1)} + \Omega^{(2)} \beta \Delta\mu \right) [\Phi'(\Theta) - \Phi'(0)],$$

$$W^{(1)} \approx \Lambda^{(0)} / \beta + \Lambda^{(1)} \Delta\mu.$$

Here, Φ' represents the derivative of the inside potential Φ with respect to θ , and the coefficients $\Omega^{(i)}(V)$ and $\Lambda^{(i)}(V)$ are functions of the inside potential depth V . They are expressed as

$$\Omega^{(0)} = \frac{\sinh(\beta V/2)}{1 + \cosh(\beta V/2)},$$

$$\Omega^{(1)} = \frac{1}{4 \cosh^2(\beta V/4)},$$

$$\Omega^{(2)} = \frac{e^{\beta V/2} (e^{\beta V/2} - 1)}{(e^{\beta V/2} + 1)^3},$$

and

$$\Lambda^{(0)} = \int_0^{2\pi} d\theta \left[\frac{\beta \Phi'(\theta)}{2 \cosh[\beta (\Phi(\theta) - \langle \Phi \rangle) / 2]} \right]^2,$$

$$\Lambda^{(1)} = \int_0^{\Theta} d\theta \frac{[\beta \Phi'(\theta)]^2 e^{\beta(\Phi(\theta) - \langle \Phi \rangle)} (e^{\beta(\Phi(\theta) - \langle \Phi \rangle)} - 1)}{(e^{\beta(\Phi(\theta) - \langle \Phi \rangle)} + 1)^3}.$$

The overall free energy change of the motor and the two reservoirs is expressed as

$$\Delta F = W_{\text{net}} - T \Delta S^{(\text{ir})},$$

with Eqs. (C1) and (C2), we obtain the irreversible entropy production as

$$\Delta S^{(\text{ir})} \approx \frac{2\pi(2\pi\gamma + \tau_r \Lambda^{(0)} / \beta)}{\tau_{\text{cycle}}},$$

which is inversely proportional to the cycle time τ_{cycle} , indicating that our model represents a low dissipation chemical engine [22, 25].

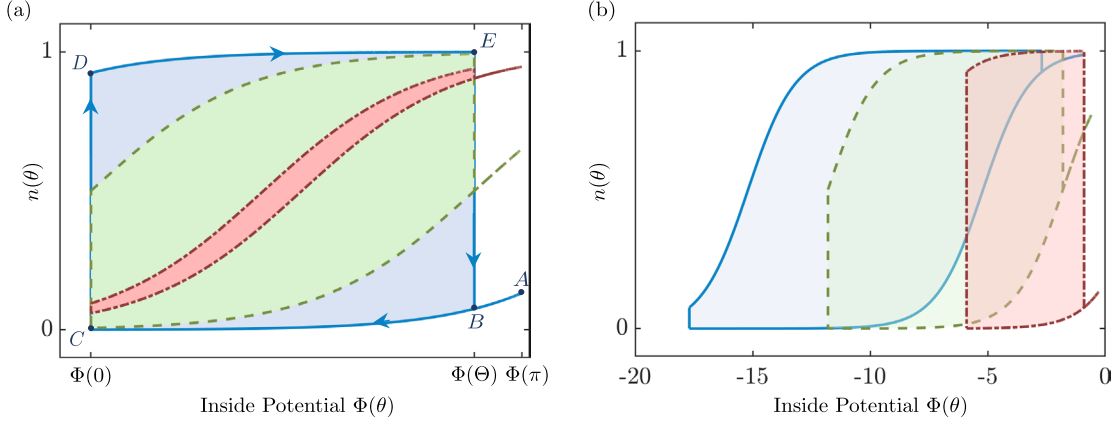


Figure 6. $n - \Phi$ diagram for quasi static cycles. (a) Cycles with different chemical potential differences: $\Delta\mu = 10k_B T$ (blue solid curve), $\Delta\mu = 5k_B T$ (green dashed curve) and $\Delta\mu = 0.5k_B T$ (red dash-dotted curve). The IPD is fixed as $V = 5k_B T$ (b) Cycles with different IPDs: V with values of $V = 15k_B T$ (blue solid curve), $V = 10k_B T$ (green dashed curve), and $V = 5k_B T$ (red dash-dotted curve). The chemical potential difference is fixed as $\Delta\mu = 10k_B T$.

Now we consider (C2) with the positive work condition of $W_{\text{net}} > 0$. There is

$$\omega < \frac{W^{(0)}}{2\pi\gamma + \tau_r W^{(1)}} = \frac{\Omega^{(0)}\Delta\mu}{2\pi\gamma + \tau_r (\Lambda^{(0)}/\beta + \Lambda^{(1)}\Delta\mu)}$$

$$\approx \frac{\Omega^{(0)}}{2\pi\gamma + \tau_r \Lambda^{(0)}/\beta} \Delta\mu.$$

Thus, with given frictional coefficient γ , the positive work condition ensures that $\omega\tau_r\Delta\mu$ is a higher-order infinitesimal with respect to $\Delta\mu$, i.e., $\omega\tau_r\Delta\mu \sim O(\Delta\mu^2)$. Therefore, the assumption $\omega\tau_r \rightarrow 0$ for $\Delta\mu \rightarrow 0$ is consistently validated within our framework.

The efficiency η is then obtained as

$$\eta = \frac{W_{\text{net}}}{\Delta\mu\Delta n} = \frac{\Omega^{(0)}\Delta\mu - \omega(2\pi\gamma + \tau_r\Lambda^{(0)}/\beta + \tau_r\Lambda^{(1)}\Delta\mu)}{(\Omega^{(0)} + \Omega^{(1)}\beta\Delta\mu)\Delta\mu},$$

$$\approx \frac{\Omega^{(0)}\Delta\mu - \omega(2\pi\gamma + \tau_r\Lambda^{(0)}/\beta)}{\Omega^{(0)}\Delta\mu}. \quad (\text{C3})$$

With the approximation to the leading order, the power is obtained as

$$P \approx \frac{\omega}{2\pi} \left(\Omega^{(0)}\Delta\mu - \omega(2\pi\gamma + \tau_r\Lambda^{(0)}/\beta) \right). \quad (\text{C4})$$

With Eqs. (C3) and (C4), ω is canceled, resulting in

$$P = \frac{\Delta\mu^2}{2\pi} \frac{[\Omega^{(0)}(V)]^2}{2\pi\gamma + \Lambda^{(0)}(V)\tau_r/\beta} \eta(1 - \eta).$$

Eqs. (9) and (10) are derived by optimizing the IDP V to achieve a maximum P with respect to the specific efficiency η .

Within such an LR regime, the rotation speed at maximum power is obtained as

$$\omega^* \approx \frac{\Omega^{(0)}\Delta\mu}{2(2\pi\gamma + \tau_r\Lambda^{(0)}/\beta)}.$$

Hence, the average particle exchange rate between the two reservoirs is linear with respect to the chemical potential difference, i.e.,

$$J \equiv \omega\Delta n/2\pi \approx \frac{[\Omega^{(0)}]^2}{2(2\pi\gamma + \tau_r\Lambda^{(0)}/\beta)} \Delta\mu \propto \Delta\mu.$$

The average effect of the steady rotation for the motor generates a current whose response is linear with respect to the driving $\Delta\mu$ [25, 27, 41].

* hdong@gscaep.ac.cn

- [1] K. Huang, *Statistical mechanics*, 2nd ed. (Wiley, New York, 1991).
- [2] L. Chen, F. Sun, C. Wu, and J. Yu, *Energy Convers. Manag.* **38**, 1841 (1997).
- [3] T. Schmiedl and U. Seifert, *EPL* **81**, 20003 (2007).
- [4] S. Sieniutycz, *Int. J. Heat Mass Transf.* **51**, 5859 (2008).
- [5] S. Amano, S. Borsley, D. A. Leigh, and Z. Sun, *Nat. Nanotechnol.* **16**, 1057 (2021).
- [6] H. Hooyberghs, B. Cleuren, A. Salazar, J. O. Indekeu, and C. Van den Broeck, *J. Chem. Phys.* **139**, 134111 (2013).
- [7] M. P. Leighton and D. A. Sivak, *Phys. Rev. Lett.* **130**, 178401 (2023).
- [8] M. P. Leighton and D. A. Sivak, (2024), [arXiv:2406.10355 \[cond-mat.stat-mech\]](https://arxiv.org/abs/2406.10355).
- [9] P. Dimroth, H. Wang, M. Grabe, and G. Oster, *PNAS* **96**, 4924 (1999).
- [10] D. D. Hackney and F. Tamanoi, *The enzymes.*, 3rd ed. (Elsevier Academic Press, Amsterdam, 2004).
- [11] C. Von Ballmoos, A. Wiedenmann, and P. Dimroth, *Annu. Rev. Biochem.* **78**, 649 (2009).
- [12] R. Phillips, *Physical biology of the cell*, second edition ed. (Garland Science, London : New York, NY, 2013).
- [13] R. Rao and M. Esposito, *Phys. Rev. X* **6**, 041064 (2016).

- [14] M. R. Wilson, J. Solà, A. Carlone, S. M. Goldup, N. Lebrasseur, and D. A. Leigh, *Nature* **534**, 235 (2016).
- [15] S. Amano, M. Esposito, E. Kreidt, D. A. Leigh, E. Penocchio, and B. M. W. Roberts, *Nat. Chem.* **14**, 530 (2022).
- [16] E. Lathouwers and D. A. Sivak, *Phys. Rev. E* **105**, 024136 (2022).
- [17] S. Borsley, E. Kreidt, D. A. Leigh, and B. M. W. Roberts, *Nature* **604**, 80 (2022).
- [18] A. Singh, J. A. Soler, J. Lauer, S. W. Grill, M. Jahnel, M. Zerial, and S. Thutupalli, *Nat. Phys.* (2023), 10.1038/s41567-023-02009-3.
- [19] F. L. Curzon and B. Ahlborn, *Am. J. Phys.* **43**, 22 (1975).
- [20] C. Van den Broeck, *Phys. Rev. Lett.* **95**, 190602 (2005).
- [21] Z. C. Tu, *J. Phys. A: Math. Theor.* **41**, 312003 (2008).
- [22] M. Esposito, R. Kawai, K. Lindenberg, and C. Van den Broeck, *Phys. Rev. Lett.* **105**, 150603 (2010).
- [23] J. Lin, S. Xie, C. Jiang, Y. Sun, J. Chen, and Y. Zhao, *Sci. China Ser. E* **65**, 646 (2021).
- [24] V. Holubec and A. Ryabov, *J. Stat. Mech: Theory Exp.* **2016**, 073204 (2016).
- [25] V. Holubec and A. Ryabov, *Phys. Rev. E* **96**, 062107 (2017).
- [26] V. Holubec and A. Ryabov, *Phys. Rev. Lett.* **121**, 120601 (2018).
- [27] K. Proesmans, B. Cleuren, and C. Van den Broeck, *Phys. Rev. Lett.* **116**, 220601 (2016).
- [28] N. Shiraishi, K. Saito, and H. Tasaki, *Phys. Rev. Lett.* **117**, 190601 (2016).
- [29] P. Pietzonka and U. Seifert, *Phys. Rev. Lett.* **120**, 190602 (2018).
- [30] Y.-H. Ma, D. Xu, H. Dong, and C.-P. Sun, *Phys. Rev. E* **98**, 042112 (2018).
- [31] R.-X. Zhai, F.-M. Cui, Y.-H. Ma, C. P. Sun, and H. Dong, *Phys. Rev. E* **107**, L042101 (2023).
- [32] B. Andresen, P. Salamon, and R. S. Berry, *Phys. Today* **37**, 62 (1984).
- [33] U. Seifert, *Rep. Prog. Phys.* **75**, 126001 (2012).
- [34] F. Jülicher, A. Ajdari, and J. Prost, *Rev. Mod. Phys.* **69**, 1269 (1997).
- [35] C. Bustamante, D. Keller, and G. Oster, *Acc. Chem. Res.* **34**, 412 (2001).
- [36] H. Wang and G. Oster, *EPL* **57**, 134 (2002).
- [37] N. Golubeva and A. Imparato, *Phys. Rev. Lett.* **109**, 190602 (2012).
- [38] T. Schmiedl and U. Seifert, *EPL* **83**, 30005 (2008).
- [39] W. R. Bauer and W. Nadler, *J. Chem. Phys.* **129** (2008), 10.1063/1.3026736.
- [40] Y. Zhang, C. Huang, G. Lin, and J. Chen, *Physica A* **474**, 230 (2017).
- [41] O. Raz, Y. Subaşı, and C. Jarzynski, *Phys. Rev. X* **6**, 021022 (2016).
- [42] M. Esposito, K. Lindenberg, and C. Van den Broeck, *Phys. Rev. Lett.* **102**, 130602 (2009).
- [43] Z.-C. Tu, *Chin. Phys. B* **21**, 020513 (2012).
- [44] M. Josefsson, A. Svilans, A. M. Burke, E. A. Hoffmann, S. Fahlvik, C. Thelander, M. Leijnse, and H. Linke, *Nat. Nanotechnol.* **13**, 920 (2018).
- [45] Y. H. Chen, J.-F. Chen, Z. Fei, and H. T. Quan, *Phys. Rev. E* **106**, 024105 (2022).